Research Square

Preprints are preliminary reports that have not undergone peer review.
They should not be considered conclusive, used to inform clinical practice,
or referenced by the media as validated information.

Influence of Weld Proximity and Sequence on Residual Stress and Distortion in Friction Stir Welding: A Neutron Diffraction Study

Nicholas Sabry

nicholas@sabry-engineering.com

The University of British Columbia https://orcid.org/0000-0003-4255-3597

Dimitry Sediako

The University of British Columbia

Kirk Fraser

National Research Council Canada

Francois Nadeau

National Research Council Canada

Joshua Stroh

Australian Nuclear Science and Technology Organisation

Anna Paradowska

Australian Nuclear Science and Technology Organisation

Mark Reid

Australian Nuclear Science and Technology Organisation

Research Article

Keywords: Lap-joint welding, Friction Stir Welding (FSW), Residual Stress, Neutron Diffraction, Temperature Simulations, Multi-Welded Components

Posted Date: November 23rd, 2026

DOI: https://doi.org/10.21203/rs.3.rs-11603172/v1

License: This work is licensed under a Creative Commons Attribution 4.0 International License.
Read Full License

Influence of Weld Proximity and Sequence on Residual Stress and Distortion in Friction Stir Welding: A Neutron Diffraction Study

Author Names and Affiliations

Nicholas Sabry[a], ORCID: 0000-0003-4255-3597, nicholas@sabry-engineering.com
Corresponding author

Dimitry Sediako[a], ORCID: 0000-0002-4135-3297, dimitry.sediako@ubc.ca

Kirk Fraser[b], ORCID: 0000-0002-8998-7328, kirk.fraser@cnrc-nrc.gc.ca

Francois Nadeau[b], ORCID: 0009-0008-8322-9308, francois.nadeau@cnrc-nrc.gc.ca

Joshua Stroh[c], ORCID: 0000-0003-1607-4613, strohj@ansto.gov.au

Anna Paradowska[c], ORCID: 0000-0002-0688-8843, anp@ansto.gov.au

Mark Reid[c], ORCID: 0009-0003-0180-3016, markr@ansto.gov.au

[a] High-Performance Powertrain Materials Laboratory, University of British Columbia, 1137 Alumni Ave, Kelowna, BC, V1V 1V7, Canada

[b] National Research Council Canada, Saguenay, 501, boul. de l'Université Est, Saguenay, QC, Canada, G7H 8C3

[c] Australian Nuclear Science and Technology Organisation, Lucas Heights, New South Wales, NSW 2234, Illawarra Road Lucas Heights, Australia

Abstract

The optimization of Friction Stir Welding (FSW) processes for dissimilar aluminum alloys, such as 6061 and A365, requires a comprehensive understanding of how weld sequence and proximity impact residual stresses and distortions. This study investigates the effects of welding sequence, weld configuration, and pre-existing temperature conditions on residual stress distribution and distortion in FSW. Using neutron diffraction and coordinate-measuring machine (CMM) scanning, the study evaluates various multi-welded configurations and their residual stress fields in relation to distortion profiles. Key findings indicate that the cumulative effect of sequential welds

introduces considerable distortion, particularly when welding stages involve cooling intervals between sequences. Furthermore, torque measurements remained consistent across configurations, suggesting that initial plate temperature minimally influences torque but significantly affects the magnitude and distribution of residual stresses and distortions. Plates welded with successive sequences showed reduced tensile residual stresses at plate edges compared to those allowed to cool between welds. The implications of these findings suggest that maintaining a controlled thermal gradient by minimizing wait times between welds can effectively reduce distortion. These insights inform welding strategies for large-scale components, emphasizing the importance of thermal and residual stress management in enhancing weld quality and structural integrity.

Key Words

Lap-joint welding; Friction Stir Welding (FSW); Residual Stress; Neutron Diffraction; Temperature Simulations; Multi-Welded Components

1. Introduction

Examining the sequence and order of welds as a function of residual stress generation is an important area for optimizing Friction Stir Welding (FSW) and improving the performance and reliability of welded components in various industrial applications, yet few studies have explored this area. In FSW, heat generated by the rotating tool softens the material, which then reforms behind the tool as it advances. This process can cause residual stresses to form in the material due to thermal expansion and contraction, plastic deformation, and microstructural changes. The proximity and order of welds can affect residual stress in several ways. For example, if welds are too close together, they may overlap and create higher levels of residual stress in the material. Welding in a specific order may also affect residual stress, as current welds may interact with residual stresses generated by previous welds, leading to changes in the residual stress profile.

Research on proximity welds and their effects on residual stresses has been more prevalent in fusion welding. Bhardwaj et al. [1] investigated residual stresses in proximity girth welds using fusion welding techniques, finding that close proximity welds can significantly increase tensile residual stresses due to high constraints and multiaxial stress states. This highlights the critical nature of weld sequence and spacing in fusion welding. However, such extensive studies and set standards for proximity welds are lacking in the context of FSW. The unique characteristics of FSW, such as lower heat input and solid-state joining, necessitate specific data collection to understand how proximity and sequence of welds impact residual stresses in FSW.

Sun et al. [2] demonstrated that the number and distribution of weld seams critically influence the forming accuracy and mechanical properties of spun-formed workpieces, highlighting the need for precise control over weld placement in complex components. Martin et al. [3] developed novel techniques for corner joints using FSW, emphasizing how different joint configurations and thermal cycles impact weld quality. Agapiou and Carlson [4] explored the optimization of welding parameters for copper components in electric motors, underscoring the challenges of managing thermal effects during welding. Notably, Agapiou and Carlson's work, despite being conducted on copper rather than aluminum, provides one of the few examples of non-overlapping proximity friction stir welds on a circularly enclosed part. These aspects are both essential to industrial welding, highlighting the potential for cross-material insights and the critical need for specific studies focused on aluminum.

Residual stresses have significant effects on fatigue and distortion in welded components. Dalle Donne et al. [5] found that residual stresses are much more influential than weld quality in determining the fatigue crack propagation rates in friction stir welded joints, highlighting the importance of understanding residual stress effects. Chen and Kovacevic [6] used finite element

analysis to study stress evolution during FSW, demonstrating how residual stresses impact fatigue strength and distortion. Furthermore, Charitidis et al. [7] investigations using nanoindentation techniques demonstrate that residual stresses can lead to localized deformation and affect mechanical properties.

Therefore, a systematic investigation of the effects of welding sequence and proximity on residual stress in FSW can help optimize the welding process and minimize the detrimental effects of residual stress on the material. Hence, the present investigation aims to develop a comprehensive framework to determine the impact of welding process conditions relating to weld sequence on the formation of residual stresses in dissimilar aluminum alloy friction stir welds (i.e., 6061 joined to A365).

2. Experimental Details

2.1. Materials, Weld Process, Data Collection, and Quality Assurance

The present study utilizes a 6061 aluminum top plate welded to an A365 aluminum casting (see Figure 1). This study uses constant welding parameters to compare welding sequences and order with an additional time variable for one of the plates. As shown in Table 1, the traverse and rotational speeds were set. Testing welds were utilized on additional plates to determine the optimal plunging force by gradually increasing it until defects ceased, as verified by ultrasound. The ideal plunging force of 6.9 kN was then applied to the plates studied. To ensure industry-quality welds, each plate was scanned using ultrasound, as shown in Figure 2 with Plate I.

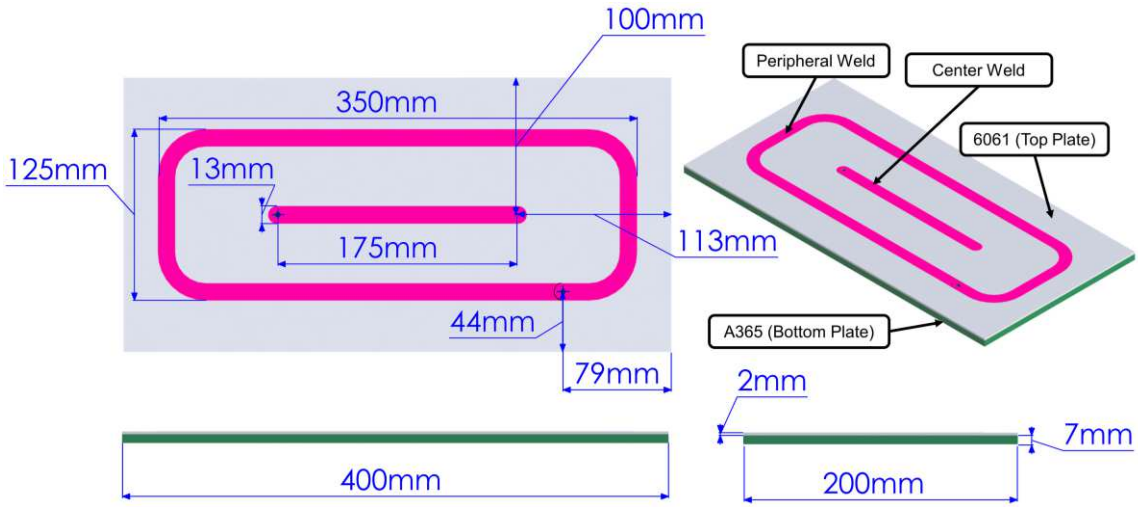


Figure 1: Lap weld configuration for welding (combined component thickness: 9 mm)

Table 1: FSW processing conditions (multi-welded plates)

Dwell Time (s)	Traverse Speed (mm/min)	Rotational Speed (RPM)	Plunge Force (kN)	Plunge Feed (mm/min)	Withdraw Feed (mm/min)
1.2	950	1500	6.9	120	250

Figure 2 displays the A-scan with amplitude readings and depth. The initial 0.4 mm shows increased noise due to the sheet surface quality rather than an ultrasound artifact. As a result, the top surface is considered to start at 0.4 mm, and any defects within this region may not be detectable.

The B-scan provides a longitudinal view of the depth, with colors corresponding to the A-scan amplitudes. The first 1 mm shows unreliable readings due to the dead zone, but below this, consistent green-yellow indicates low amplitude or near-zero readings, suggesting no significant defects. The B-scan also includes a transverse view, showing three cross-sections, two for the peripheral weld and one for the center, demonstrating good weld quality at the interfaces. The C-scan, included for completeness, outlines the top surface.

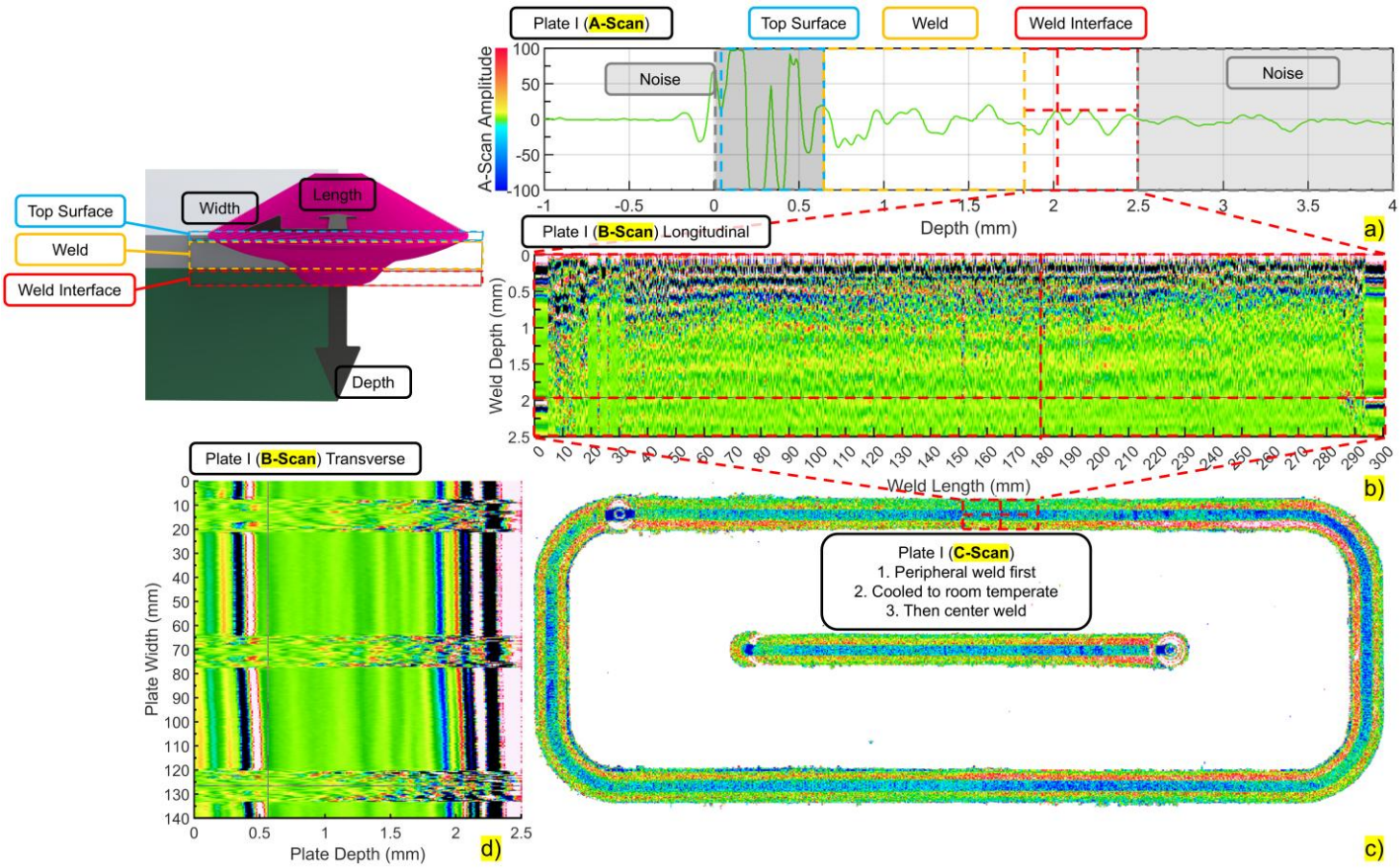


Figure 2: Ultrasonic non-destructive evaluation of friction stir welds; (a) one-dimensional display of amplitude versus depth; (b) cross-sectional view revealing defects across the length and depth; (c) external details of the weld projected onto a plane; (d) cross-sectional view revealing defects across the width and depth

The unreliability of depth readings on ultrasound in friction stir weld inspections is primarily due to surface irregularities and high-noise signals creating a dead zone. This dead zone affects the initial 1.0 mm from the surface. Nonetheless, the method remains effective for detecting deeper defects, ensuring the overall integrity of the weld can still be assessed. Ultrasonic scans were utilized to validate the weld quality of each plate and weld in this study, following the same process described in Figure 2. The final parameter requiring consideration is consistent fixturing, which is important for comparability between plates. The manner in which material is constrained during welding and released post-welding can influence distortion and residual stress. For example, Costa et al. [8] demonstrated that changing the releasing strategy from counterclockwise (CCW) to

clockwise (CW) affects residual stress and plate distortion, albeit with minor effects. Therefore, the plates in this study maintained uniformity in clamping configurations and release schedules, as shown in Figure 3.

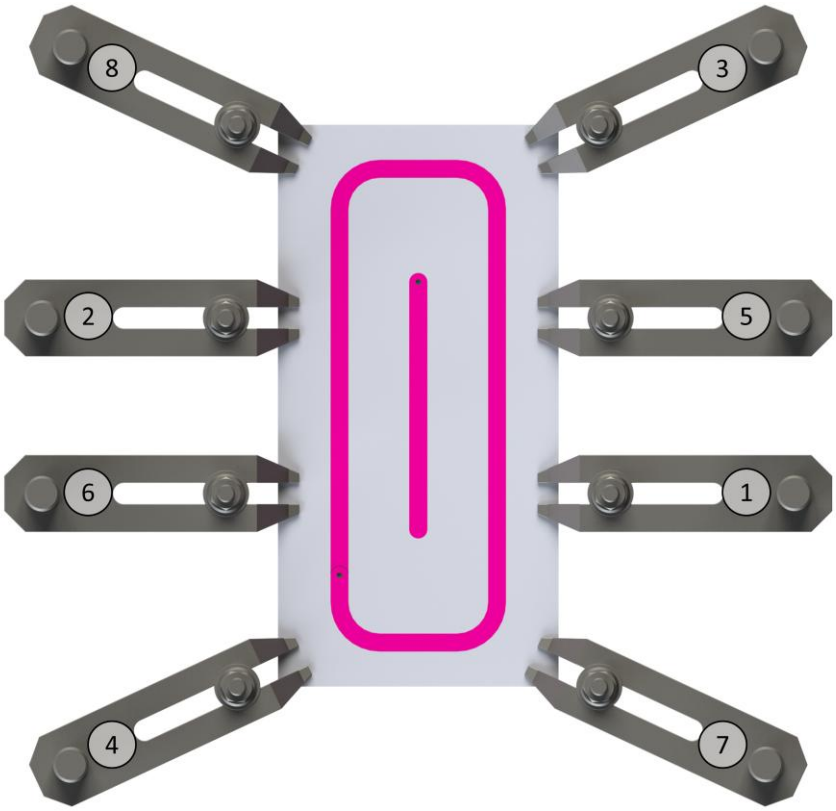


Figure 3: Rigging and releasing conditions utilized (1 start, 8 end)

2.2. CMM Distortion

The plates were scanned for distortion post-friction stir welding using a coordinate-measuring machine (CMM) system with laser feedback technology for high-precision 3D scanning and measurement. The scanner employs SHINE (Systematic High-Intelligence Noise Elimination) technology to ensure high-quality data collection on surfaces with varying reflectivity, such as the glossy material of plate 6061. A wide laser scan line covered the entire surface area of each plate, and the system's high point acquisition rate, up to 1.2 million points per second, ensured the creation of detailed and accurate 3D models for comparison to a non-distorted 3D model.

3. Results and Discussion

3.1. Distortion

There are five plates labeled E, F, G, H, and I, each welded using friction stir welding (FSW) but with different configurations. Each weld on all plates has a uniform bead width of 13 mm. Plate E features a single central weld 175 mm long. Plate F includes a circular peripheral weld encircling the center weld, measuring 350 mm long and 125 mm wide (see Figure 1). Plate G incorporates a central weld followed by a peripheral weld, whereas Plate H is welded peripherally first and then centrally. Plate I differs in that after the peripheral weld, it is cooled to ambient temperature before the central weld is applied (see Figure 4 for weld order). Distortion measurements were taken using a coordinate measuring machine (CMM) from a flat cad reference model. Distortion on a 400 mm long plate ranges from +1 mm to -1 mm depending on weld configuration, indicating noticeable changes considering the component's thickness (see Figure 1). While joint configuration plays a significant role, the exact degree of distortion depends on various factors, including the specific welding parameters, fixture setup, and the welded materials. Therefore, making direct comparisons or drawing conclusions between different studies can be unrealistic due to these variables.

Specifically, Plate E shows negligible distortion at the start of the central weld, intensifying to -1 mm distortion toward only the end of the weld (see Figure 4). Plate F, which features only the peripheral weld and lacks a center weld (see Figure 4), displays notable distortion. Specifically, significant portions in the center of the plate show distortion at -1 mm, while the top left and bottom right corners exhibit distortions ranging from 0.75 mm to 1 mm, respectively. These differences in distortion are significant and can be attributed to the difference in bulk material support at the plate's edges and the considerably longer weld path of the peripheral weld compared to a configuration with only a center weld. Plate G, which completes the center weld first and then

the peripheral weld directly after, exhibits significant distortion at -1 mm in the central areas covering large areas of the plate, with the top left and bottom right corners reaching up to +1 mm of distortion. The arrangement of the welds on Plate G, starting with the center followed by the peripheral weld, shows that the distortion affects nearly all four corners to about 0.75 mm, with the bottom of the plate below the peripheral weld measuring distortions ranging from +0.25 to +0.5 mm across its width.

Following a pattern similar to Plate G, Plate H, which reverses the welding sequence by performing the peripheral weld first and then the center weld immediately afterward, exhibits positive distortion across the entire width of the plate below the peripheral weld. This similar distortion profile suggests that the welding sequence (whether peripheral or central first) may not significantly affect distortion, as the distortion magnitudes in the corners of Plates G and H are similar. However, Plate I's weld sequence, which allowed the material to cool down to ambient temperature between welds, shows the most considerable distortion, with significant curling at the corners and more extensive negative distortion across the center toward the top left corner of the plate. This distortion profile suggests that temperature plays a fundamental role in FSW; if a component cools between welds or is performed in separate stages, the distortion profile can vary significantly, even if the welding sequence remains the same. Most notably, considering the entire data set, single welds tend to cause minimal distortion, but adding multiple welds or allowing for cooling between welds increases distortion significantly. This observation will be further explored in subsequent parts of the study to understand the effects of interacting residual stress fields and temperature variations.

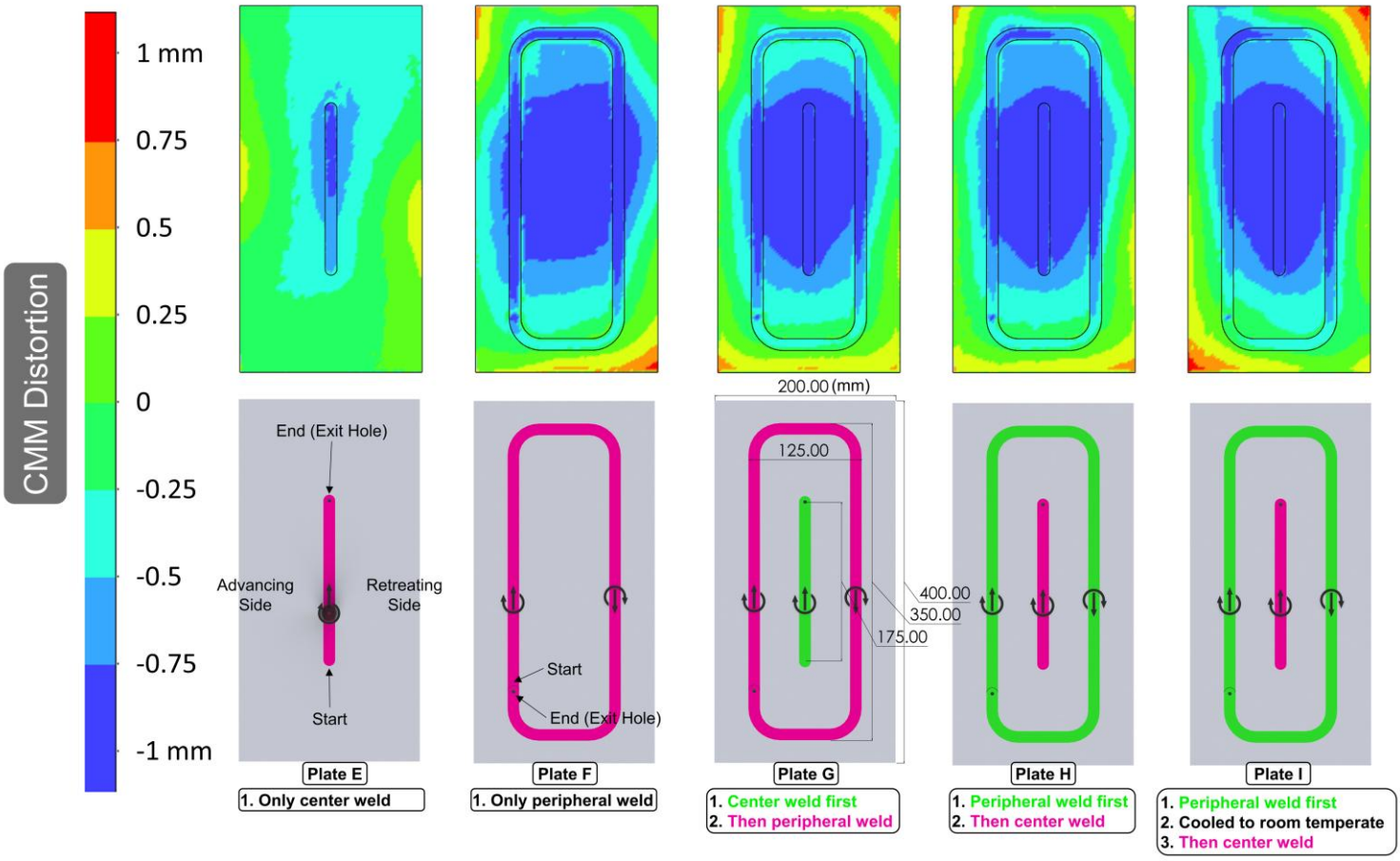


Figure 4: Coordinate measuring machine distortion (CMM) images of multi-welded plates

Distortion observed in the plates depicted in Figure 4 typically manifests as a combination of angular and bending distortions, mainly due to variations in the thermal field, material displacement, and longitudinal residual stresses throughout the plate's thickness. In thicker plates, achieving uniform conditions through the plate's thickness is increasingly difficult, a challenge often compounded by significant through-thickness temperature gradients. Xu et al. [9] identified these gradients as the primary drivers of residual stresses across the plate's thickness in FSW. Another form of distortion, buckling, results directly from the loads imposed by welding-induced residual stresses. As Williams et al. [10] remark, the applied weld load refers to the load generated by the residual stresses induced during the welding process. These residual stresses, particularly the compressive residual stresses in the outer regions of the welded plates, create a force or load

on the structure. This load can cause various forms of distortion, including buckling if it exceeds the critical buckling load of the plates. The magnitude of this critical load is influenced by the stiffness and geometry of the plates, with thinner and narrower plates having a lower threshold for buckling (Williams et al. [10]). The specific buckling mode determines the final distortion's level and shape, which can often resemble bending distortion, making it easy to confuse the two. However, the origins and management strategies for buckling and bending distortions differ. Buckling direction can be highly unpredictable, influenced by variables such as the orientation of pre-existing residual stresses or the clamping configuration used during the welding process (Williams et al. [10]). The CMM images (see Figure 4) and the unpredictable nature of distortion underscore the importance of minimizing distortion through optimal welding practices. For example, rigging and clamping alter the resulting distortion and residual stress studied by Staron et al. [11] and Costa et al. [8]. Nonetheless, it is recognized that these practices alone cannot wholly eliminate distortion and residual stress due to the asymmetric nature of FSW (He et al. [12]). Addressing this challenge may require a standardized process to ensure a flat multi-welded component immediately after welding. This process would include measuring distortion and residual stress based on a specific clamping and rigging setup, then designing and implementing counter-rigging tailored to offset the anticipated distortion. This method would involve pressing the component against a custom-designed rig to neutralize distortion, ensuring the component remains flat post-FSW. Certain automotive companies have adopted a similar process to enhance throughput by minimizing manufacturing costs, as managing post-welding distortion can be expensive and time-consuming. However, this process is not widely documented in literature due to its need for very specific rigging tailored to the welded component.

Nevertheless, various post-welding techniques can manage distortion if active management is unrealistic or too costly. Active distortion management refers to strategies implemented during the welding process to prevent or minimize distortion. This approach involves real-time adjustments and control measures to manage the residual stresses and deformation as they develop. The example mentioned above would be considered active management as it uses preemptive measures that involve anticipating potential distortions and implementing strategies to counteract them before they occur. Post-welding distortion management involves correcting any distortion that occurs after the welding process is complete. This approach focuses on remediation rather than prevention. For instance, the burnishing and coining post-welding techniques discussed in Sabry et al. [13].

3.2. Torque and Temperature Analysis

It's important to verify welding torques when examining weld sequencing in FSW, as torque is a key indicator of the load applied during the process and significantly influences welding quality (Shahi et al. [14]). In the current study, axial force and speed parameters were controlled, allowing torque to adjust freely. Monitoring the torque applied during the FSW process provides insight into the characteristics of the weld. Therefore, maintaining consistency in all aspects except sequence is essential; this ensures uniformity in heat generation, material softening, plasticizing, stirring action, penetration depth, and process stability across different plates. Figure 5 demonstrates that torque measurements are highly consistent regardless of the welding sequence.

This observation indicates that torque stability is maintained across different welding sequences, suggesting that effectively managing distortion may necessitate proactive and well-planned interventions rather than adjusting parameters such as torque during welding. Furthermore, within the temperature range used in the present study, torque appears unaffected by the plate's initial

temperature. However, at significantly higher preheating temperatures, on the order of several hundred degrees Celsius, Sinclair et al. [15] has shown that torque can be affected by the starting thermal condition of the plate. While this phenomenon was not observed in the present experiments, its relevance may become more prominent under larger temperature gradients and can be explored further in relation to the temperature readings shown in Figure 6.

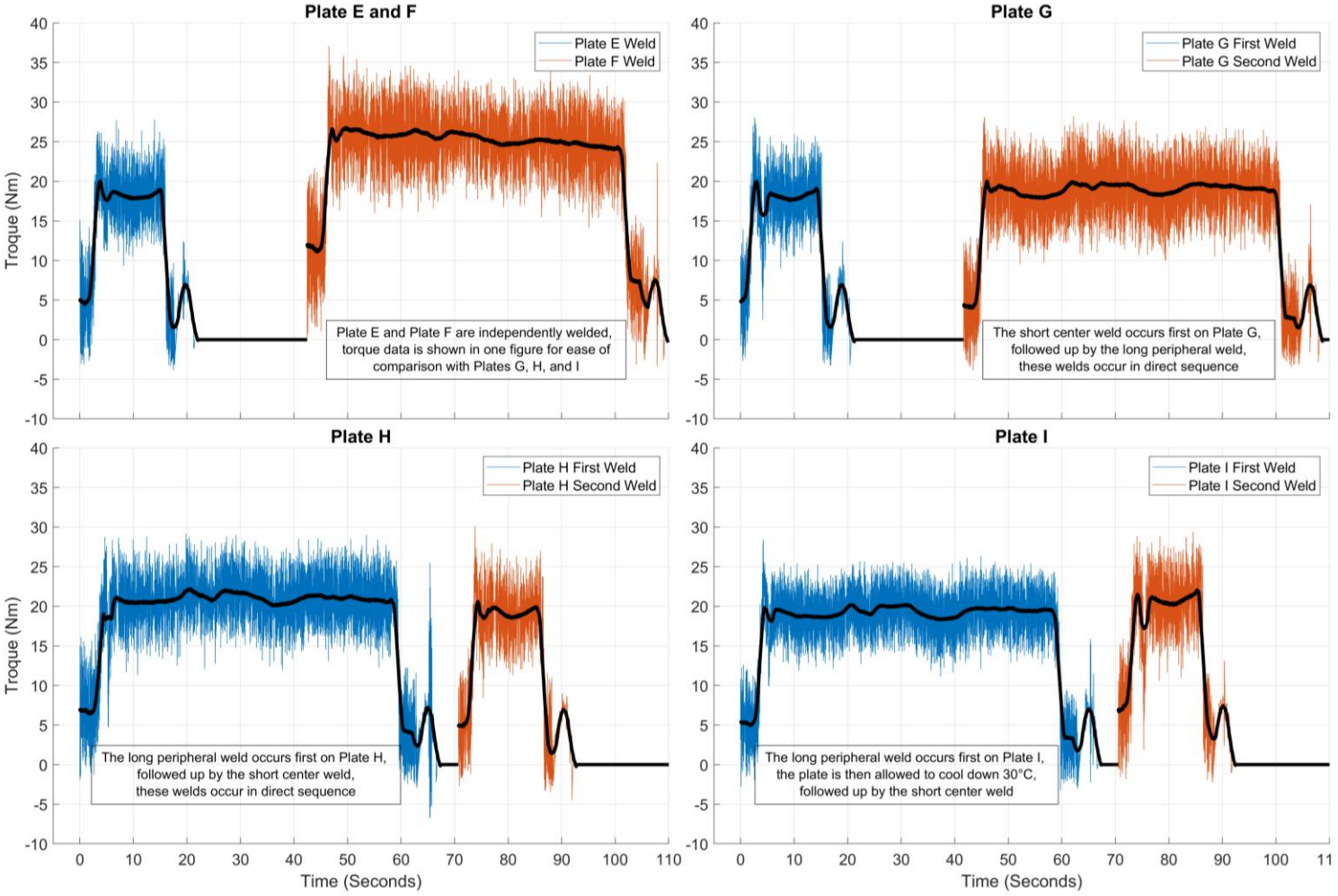


Figure 5: Spindle torque measurements during friction stir welding for each plate welded

Figure 6, featuring four thermocouples, demonstrates how the temperature generated by FSW influences the starting temperature of the plate for subsequent welds. For instance, thermocouples 1 and 2 (TC1 and TC2), both starting at nearly 25 degrees Celsius and positioned 21.5 millimeters from the edge of the 13-millimeter-wide weld seam, show similar temperature readings during the

initial center weld at the bottom end of Plate G. After completing the center weld at around the 50-second mark, the peripheral weld begins, starting and ending near the same position by the exit hole at the bottom left of Plate G. TC1, positioned on the left side, first registers a rise to 80 degrees Celsius.

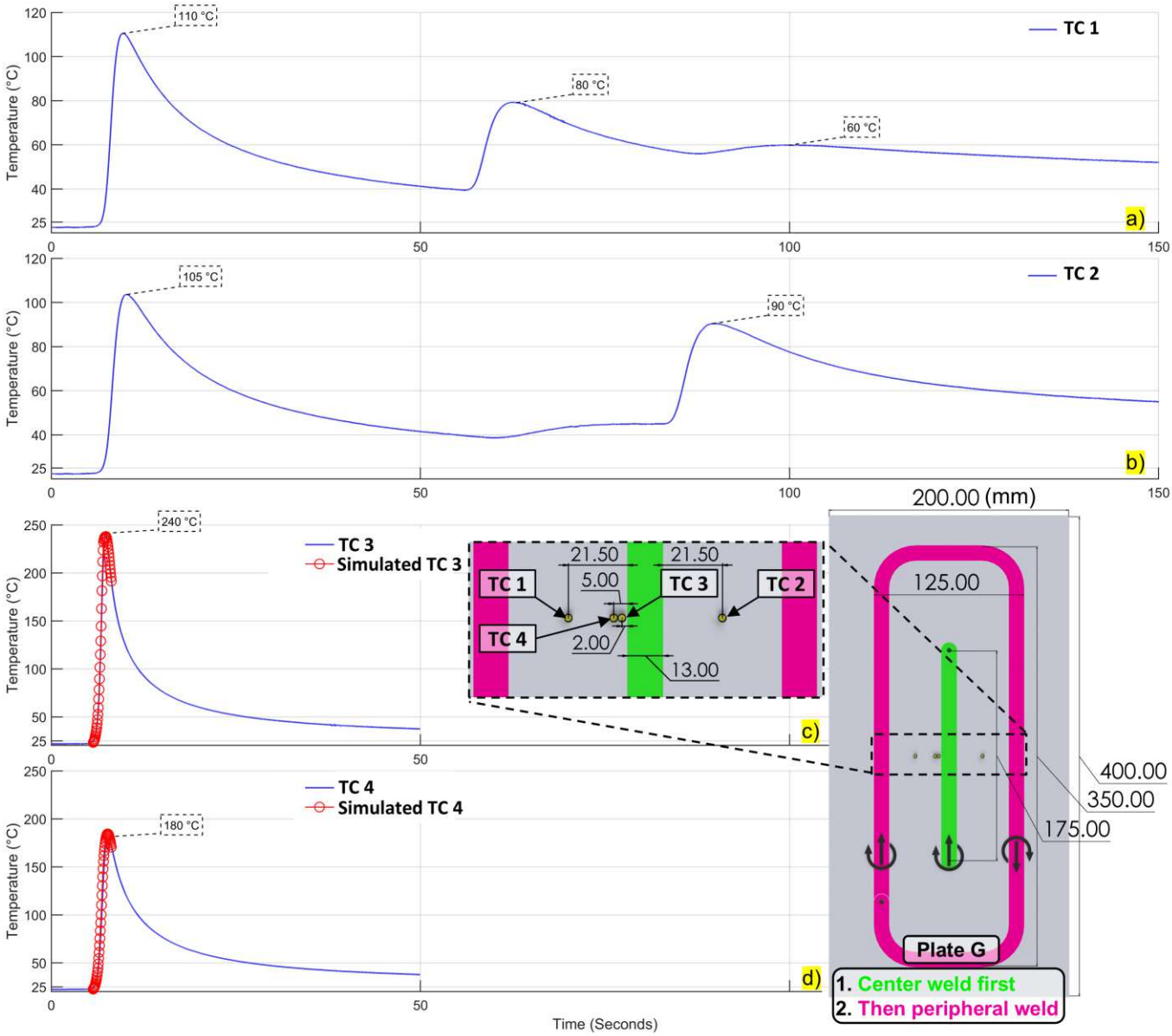


Figure 6: Measured temperature on four different thermocouples for Plate G during welding

Shortly after that, as the peripheral weld encircles the plate and the welding tool approaches the right side near TC2, the temperature at TC2 reads 10 degrees higher than the initial condition,

illustrating the additional heat introduced by the welding sequence. In cases where a weld is performed immediately after a previous weld, the starting plate temperature will be elevated. However, in the present study, that increase, below 100°C, does not appear to significantly affect the torque readings. This may explain why torque values remain relatively consistent across the different plates.

In FSW, the torque required to move the tool through the material primarily depends on material properties, tool geometry, and process parameters like rotational speed and traverse speed. The findings between Figure 5 and Figure 6 suggest that variations in starting temperature do not significantly influence the torque because the process inherently accommodates a wide range of temperatures due to friction-generated heat. This heat leads to the thermal softening of the material, which is more significant than the initial temperature in determining the torque required. Therefore, it could be hypothesized that while initial plate temperature might cause minor fluctuations in starting torque, these variations are likely overshadowed by the more substantial temperature changes and material softening caused by the welding process. This hypothesis might explain why initial temperature variations don't significantly affect torque, as any minor changes are quickly mitigated by the intense heat generated during welding, which dominates the material's response to the welding tool. This view aligns with a review article by Meyghani et al. [16] and studies completed by Sigl et al. [17] discussing methods for controlling welding temperature to ensure quality. The stability of torque despite variations in initial temperature could be due to the rapid thermal dynamics within the FSW process, where the temperature quickly reaches levels that diminish the impact of any initial temperature differences.

Moving on to TC3 and TC4, positioned just outside the weld path at two millimeters and five millimeters from the weld edge, respectively (see Figure 6), these thermocouples register much

higher temperatures. TC3 reaches a maximum of 240 degrees Celsius, while TC4 peaks at 180 degrees Celsius, highlighting a significant temperature decay rate between them. The data from these thermocouples are explicitly used to validate the SPH simulation data. As depicted in Figure 6c and Figure 6d, TC3 and TC4 are strategically placed to capture essential temperature gradients across the weld area, just outside the direct influence of the welding tool. The setup for TC3 and TC4 allows for a comparison of real-world temperature readings with the simulation, ensuring that the SPH model accurately replicates the thermal dynamics of FSW and reinforcing the model's validity and reliability. Figure 7 depicts a specific material segment being tracked over time, creating a temperature contour in Figure 8. As the simulation progresses, the FSW tool approaches and physically interacts with the analyzed material segment, displacing material points and resulting in a blank spot (see Figure 7 and Figure 8) on the temperature data map at the point of material displacement, which is subsequently refiled.

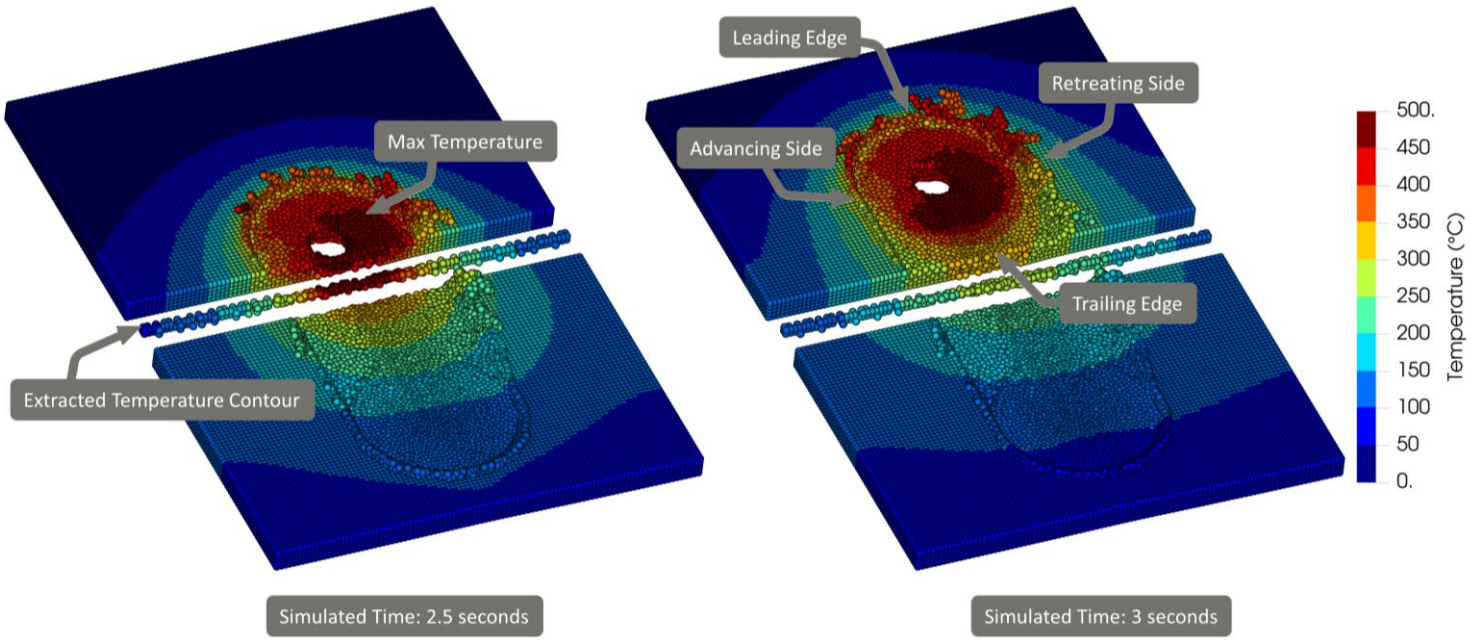


Figure 7: SPH simulation of center friction stir weld

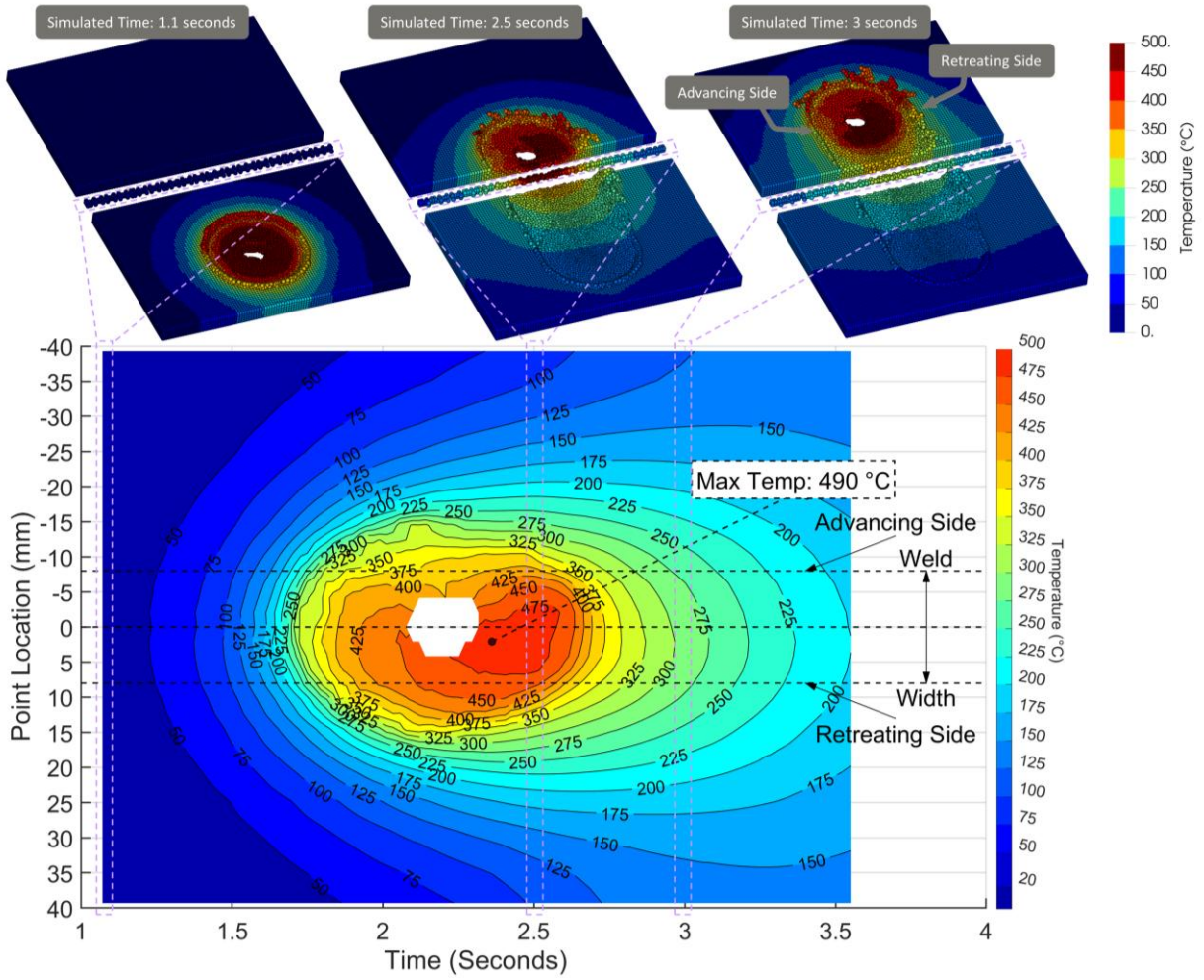


Figure 8: Temperature contour illustrating the thermal gradients of the stationary material over the simulation period for friction stir welded

The contour image (Figure 8) does not represent the traverse or rotational direction of the tool in any physical sense. Instead, it records and displays the temperature at a specific, fixed location of material over time (see Figure 7). At time zero, the material is at a constant room temperature. The simulation does not include a plunging phase; it begins at 1.1 seconds. The first recorded 'simulation time' is 0.02 seconds, which, when multiplied by the velocity scaling factor of 50 (as defined in the simulation), results in 1.07 seconds. This marks the actual start of the simulation, not zero.

The velocity scaling factor is used to expedite the simulation, calculating only a fraction of the actual time in 'simulation time' and then multiplying the result by the velocity scaling factor to obtain 'real-time.' Fraser [18] explains that this is achieved using velocity scaling (or time scaling), which does not alter the time step size. Instead, it allows more simulation to be performed in a reduced timeframe by scaling all relevant terms by a velocity scaling factor. These terms include rotational speed, traverse speed, thermal conductivity, convection coefficient, and other related parameters. It is essential to exercise caution when applying this method, as Fraser [18] emphasizes, to ensure that the system's dynamics are not unreasonably altered.

Notably, in Figure 8, the maximum temperature consistently occurs at the trailing edge of the FSW process, which lies on the retreating side of the tool. This finding aligns with Silva-Magalhães et al. [19] measuring maximum temperature on the retreating-trailing edge of the FSW tool. This area reaches a maximum temperature of 490 °C, which is significant yet still below the melting point of aluminum, with the solidus temperature for 6061 and A365 at 590 °C and 570 °C respectively (Jin et al. [20]; Hernandez et al. [21]). The maximum temperature of 490 °C from the simulation is consistent with other physical measurements recorded by researchers in previous studies (Tang et al. [22]). Lastly, thermocouples placed 21.5 millimeters from the weld's edge, as shown in Figure 6, register temperatures around 100 degrees Celsius. The thermocouple measurements correlate well with the simulated maximum temperatures occurring approximately 30 millimeters from the center on both the positive and negative sides of the weld, reaching between 100 and 125 degrees Celsius. Heat distribution throughout the plate is evident as the simulation advances, potentially impacting subsequent welds nearby. Instead of starting at the typical 20-25 degrees Celsius for new welds, the starting temperature in the area increases to about 80 to 100 degrees Celsius due to lasting heat from previous welds. This approximately 60-degree increase from the initial

conditions could significantly influence the thermal dynamics and quality of subsequent welding processes in the vicinity.

The temperature differences resulting from the initial weld sequence significantly impact the distortion observed in Plates G, H, and I (see Figure 4). Plates G and H, although exhibiting some variances in distortion, with Plate H showing more pronounced negative distortion at minus one millimeter near the peripheral weld and Plate G displaying localized negative distortion at the center, both follow a similar welding sequence. This sequence involves one weld heating the plate, followed immediately by a second weld, whether peripheral or center. In contrast, Plate I demonstrate greater negative distortion near the top left of the plate and significant positive distortion where the plate tips curl upwards. This pronounced curling occurs because, unlike Plates G and H, Plate I undergoes a cooling period to ambient temperature between the first peripheral weld and the subsequent center weld. The higher starting temperatures for the second weld in Plates G and H, which do not cool down between welds, seem to mitigate distortion compared to Plate I, where the cooling period leads to increased distortion. This observation suggests that maintaining a higher temperature between sequential welds can reduce distortion. In industrial applications, especially with larger components, it might be beneficial to perform all welds on one section of a component consecutively before allowing any cooling. The increase in the initial starting temperature of 60 °C appears to reduce the resulting distortion. Additionally, reducing the time between welds could offer significant advantages, ensuring rapid transitions from one weld to the next without lengthy pauses. This approach could be particularly important when tool changes are necessary. These initial findings open various avenues for further exploration and adjustment in welding practices to optimize outcomes and reduce distortion in larger industrial components. As demonstrated in the study by Sinclair et al. [15], preheating the workpiece before

FSW can significantly reduce axial forces, provided the system allows these forces to vary. Notable reductions are observed in the 80 to 100 °C range, with maximum reductions of up to 43% at a preheated temperature of 200 °C. This reduction in axial force enhances material flow and improves welding quality. By incorporating preheating techniques, it is possible to achieve more consistent and reliable welding results, minimizing distortion and enhancing the overall structural integrity of welded components.

Furthermore, the initial starting temperature of subsequent welds may significantly affect residual stresses, which in turn contribute to distortion. Residual stresses, being the stresses that remain in the material after welding, are a primary cause of distortion. The temperature gradient in FSW is a critical factor in determining how the material around the weld zone experiences thermal expansion and contraction. When the initial temperature of the plate is elevated due to a previous weld, the second weld starts at a higher baseline temperature. This results in an altered temperature gradient as the tool passes through because the surrounding material's temperature is now different from what it would be if starting from ambient temperature. Residual stresses in FSW are primarily formed during the cooling phase when the material tries to contract but is restrained by the surrounding cooler, unyielded material. The contraction behavior changes if the initial temperature is higher, particularly in areas away from the immediate weld zone. This modified contraction can result in more complex residual stress patterns due to the differences in thermal contraction across the weld area. Essentially, the non-uniform cooling rates across the weld influence the magnitude and distribution of these stresses. These changes in stress formation could lead to welds with different mechanical properties or increased susceptibility to defects such as cracking or porosity, especially if the residual stresses exceed the material's strength limits. Understanding these dynamics could be important in predicting and mitigating potential weaknesses in the weld.

Therefore, controlling the initial temperature and managing the welding sequence is critical in practice. Techniques such as pre-heating or controlled cooling might ensure more uniform temperature gradients and minimize the impact on residual stress. Raising the initial temperature by preheating the component before FSW could be advantageous. Additionally, applying post-weld thermal insulation, such as a thermal blanket or a cooling chamber, can reduce temperature gradients and allow for more even and gradual cooling. However, the specific benefits of these techniques on residual stress and distortion should be investigated further.

3.3. Residual Stress

Figure 9 details the locations where residual stress measurements were taken using neutron diffraction scans. These measurements involve comparing neutron diffraction data from both stress-free and stressed samples. The stressed samples are the plates themselves, while the stress-free samples are a set of matchsticks cut from each welded subsection. These samples are spaced 2 mm apart over a distance of 200 mm, covering the dynamically recrystallized zone (DXZ), the thermomechanically affected zone (TMAZ), the heat-affected zone (HAZ), and the base material. This setup provides a stress-free reference for each material type encountered in FSW, as elaborated in the previous work of Sabry et al. [23] and Sabry et al. [24] which includes specific methods utilized to calculate residual stress for the current study.

The present section focuses primarily on the residual stress results rather than the specifics of the calculations and the use of stress-free samples, which are extensively covered in earlier sections. Figure 9 illustrates three lines on each plate for measurement: a blue line at 0 millimeters, a red line at 80 millimeters, and a green line at 160 millimeters. While the spacing between these points may vary slightly across different plates to optimize beam time, each point undergoes measurement in three directions: longitudinal (parallel to the weld), transverse (perpendicular to

the weld), and normal (perpendicular to the surface). Additionally, Figure 9 highlights the negative and positive directions relative to the advancing and retreating sides of the weld, respectively. Small icons within Figure 9 indicate the direction of tool travel and rotation, helping to identify the advancing side for each weld.

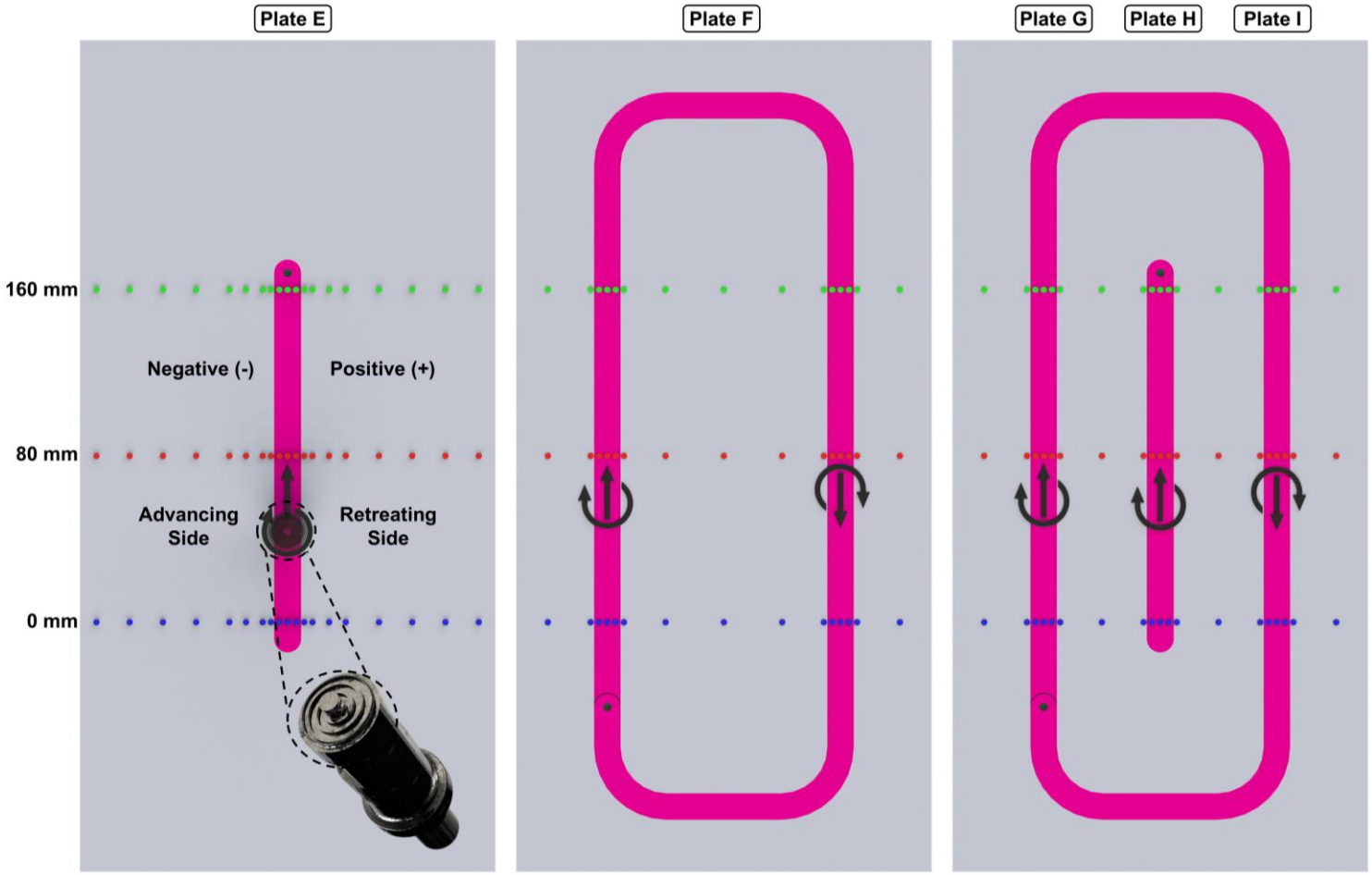


Figure 9: Blue line (0 mm line); Red line (80 mm line); Green line (160 mm line); layout for residual stress analysis on each plate

Figure 10 presents the residual stress data for plates E and F along the zero-millimeter line in the longitudinal direction. The top-left of Figure 10 consolidates the residual stress measurements of Plates E and F for easier comparison with Plates G, H, and I. Plate E shows significantly higher residual stresses on the advancing side compared to the retreating side at the start of the plate, with a 50 MPa difference and the lowest stress point at 76 MPa in the dynamically recrystallized zone (DXZ) at the center of the weld bead. This asymmetrical "M" shaped distribution is typical in

friction stir welds, influenced by composition, texture, and temperature gradients that ultimately affect the yield strength in different weld locations.

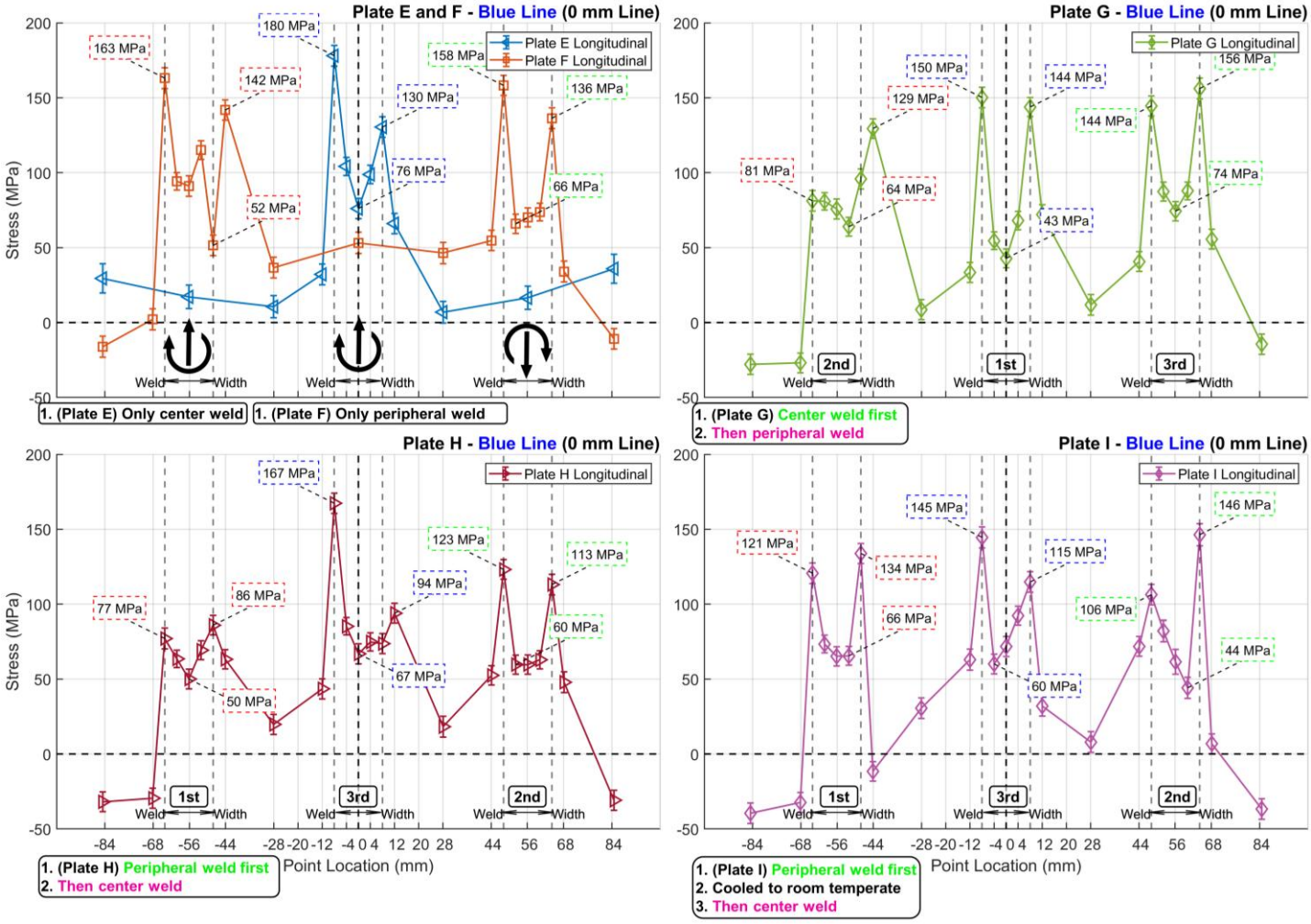


Figure 10: Blue line (0 mm line) (see Figure 9); Stress Direction: Longitudinal

At the weld edge on the advancing side near the TMAZ and HAZ interface, the maximum value of residual stress (180 MPa; see Figure 10 Plate E) is expected to coincide with the local yield strength properties. Any thermo-mechanical loading above this level is released into plastic deformation (distortion). The yield strength of A6061 is typically 240 MPa in the T6 condition, but near the weld, the strengthening is removed when the material experiences high welding temperatures.

In Plate F, which features only a peripheral weld encircling the plate, there is a distinct, albeit less pronounced, asymmetrical M-shape. The stresses on both advancing and retreating sides are closer together, illustrating less disparity in the "M" shape, indicative of interacting residual stress fields and varying temperature gradients due to the weld's circumnavigation around the periphery of the plate. The peripheral weld's interaction at the 56-millimeter mark shows closer residual stress levels between the advancing and retreating sides, differing from the typical pattern where the advancing side exhibits maximum stress in the single center welds like Plate E. The distortion measurements in Figure 4 indicate substantial differences between Plates E and F. Plate F exhibits more pronounced negative distortion at the center, with the top left and bottom right corners showing positive curling. This pattern correlates with lower residual stresses observed in these areas, suggesting that interacting residual stress fields contributed to distortion. According to Radaj [25], the temperature and microstructural state fields in welding are coupled to the stress and deformation fields affected by thermal and transformation stress, respectively. As the material distorts, it may partially relieve these stresses, only to develop new residual stress patterns influenced by the temperature distribution and the material's deformation history. Plate F, which lacks a center weld but includes a peripheral weld (see Figure 4), has significantly different distortion and longitudinal residual stress patterns in Figure 10. Maximum tensile residual stresses are lower in Plate F compared to Plate E, possibly because the edges of Plate F, with less material support due to the location of the welds, cannot sustain the imposed stress and thus release it through deformation. In Plate F, the central areas between the welds at the 0 mm location show lower residual stresses, but the difference is not as pronounced as in Plate E, where residual stresses outside the weld approach zero on both sides of the center weld. However, near the edges of Plate F, the stress state shifts into compression, particularly at points -84 and 84 millimeters. While the

tensile residual stresses are reduced for Plate F, the breath of stress extends into the compressive region, and the center exhibits elevated tensile stresses, possibly due to the interaction of residual stress from adjacent welds. This results in greater compressive stress responses near the plate's edges, which may contribute significantly to the larger distortions measured in Plate F (see Figure 4). This greater compressive stress response is not unique to Plate F. On Plates G, H, and I, each with both welds, a shift to compression near the plate's edge is observed.

Plate G's longitudinal stress profile, as depicted in Figure 10, features a center and peripheral weld, with the welding sequence starting on the center weld followed by the peripheral weld. These are detailed in the annotations as the first, second, and third welds, respectively. Although the second and third welds are part of a single circular peripheral weld, they are segmented in the figure to clarify the sequence of operations. The center weld in Plate G shows lower and nearly equal tensile stresses between the advancing and retreating sides, unlike the standalone center weld on Plate E. This difference is likely due to the temperature interactions and the influence of residual stress fields from the subsequent peripheral weld. The welds on Plate G located at the negative 56-millimeter mark (second in sequence) and the positive 56-millimeter position (third in sequence) are affected by the heat from the initial center weld. This heat generation elevates the plate's temperature, altering the temperature gradients during cooling and impacting the residual stress levels measured.

In Plate H, the welding sequence begins with the peripheral weld, reversing the order used in Plate G. When comparing Plates G and H in Figure 10, where the sequence of welds is the only variable, it is observed that Plate H exhibits lower tensile residual stresses throughout the peripheral weld. Additionally, there is a notable difference in tensile stresses between the advancing and retreating sides in the center weld. This difference demonstrates that the sequence in which the welds are

performed influences the effects on the initial weld. Specifically, in Plate H, there are lower tensile stresses on the peripheral weld closer to the end of the plate but higher maximum tensile stress in the middle. This alteration in stress distribution could impact the component's life. If changing the welding order can reduce high tensile stresses on the weld near the plate's edge, where there is less material to provide support and a higher susceptibility to crack propagation, then this represents a potential advantage to completing peripheral welds first in sequence. Nonetheless, the distortion profiles of Plates G and H are similar, suggesting that the sequence may not significantly impact the overall outcome of deformation (see Figure 4).

Plate I adopts a different strategy: the peripheral weld is completed first and allowed to cool to ambient temperature before the center weld is executed. In this configuration, the peripheral weld, particularly at the negative 56-millimeter location, does not achieve the low tensile residual stress seen in Plate H despite the peripheral weld being performed first. Moreover, Plate I's center weld exhibits stress levels comparable to those in Plate G and lower than those in Plate H but shows significantly higher distortion. A comparison of the CMM measurements from Plates H and I, as shown in Figure 4, highlights these differences in distortion. Plate I displays substantial positive distortion at the top right and bottom left corners, in contrast to Plate H.

Progressing to the 80 mm position on the plate (see Figure 9, red line), a similar pattern of longitudinal residual stress is observed, as shown in Figure 11, comparable to the 0 mm position in Figure 10, where primarily the second weld influences the residual stresses of the first weld. While the overall patterns are consistent, specific points display differences in magnitude. In the steady-state region of the weld, observing areas with lower longitudinal residual stresses is typical. This occurrence is likely linked to the consistent application of heat as the welding process transitions from the initial cold start to the more thermally stable steady-state phase. Unlike the

beginning, which starts from a colder state, or the end, which might experience an abrupt cessation of heat, the steady-state region benefits from a continuous and uniform heat application. This consistent thermal gradient could be the reason for the reduction in residual stresses observed at specific points within this region.

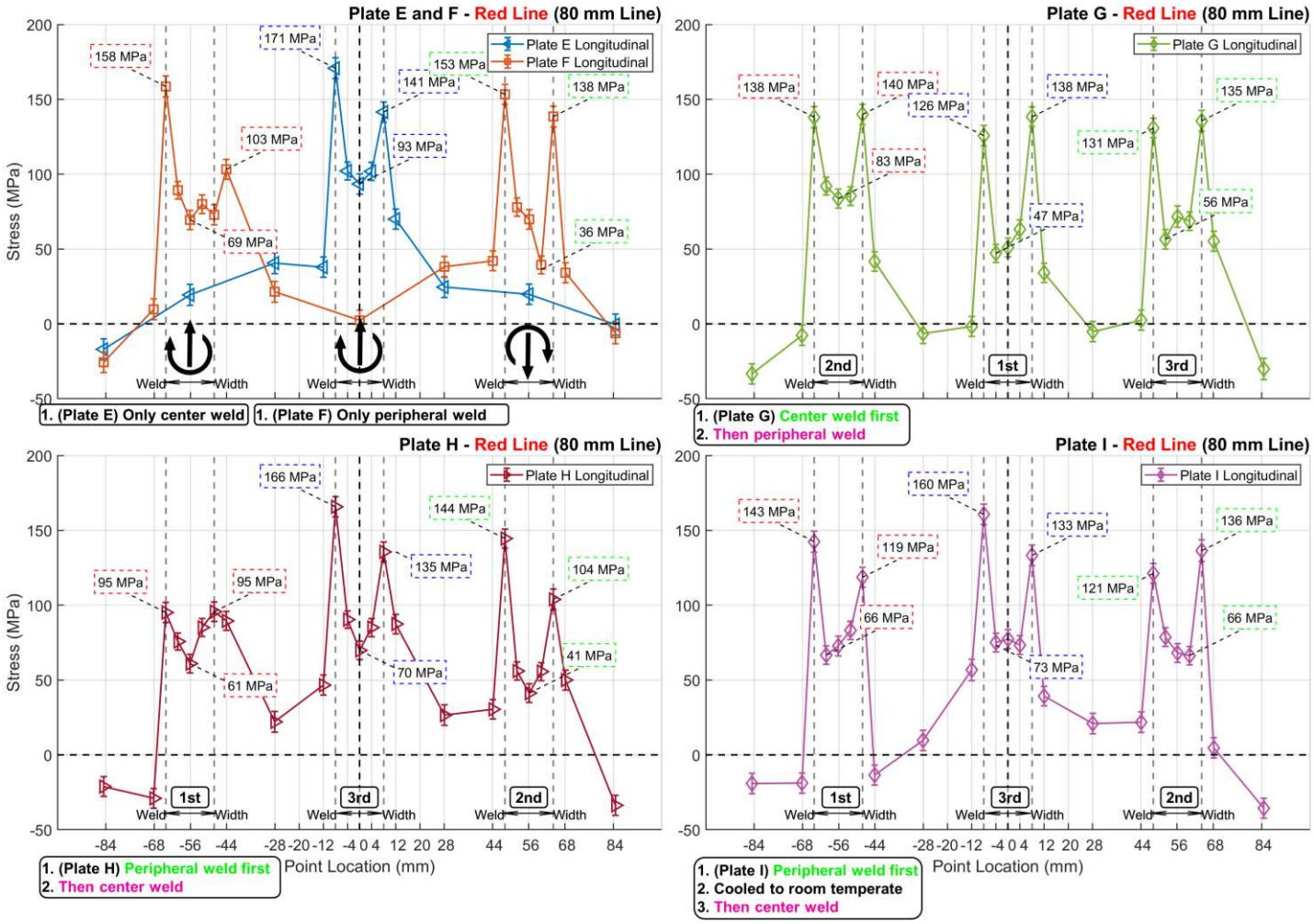


Figure 11: Red line (80 mm line) (see Figure 9); Stress Direction: Longitudinal

However, the changes in residual stress levels are not markedly pronounced across the board in Figure 11 compared to the 0 mm blue line in Figure 10. Only a few points show notable reductions. This consistent lack of magnitude reduction contrasts with single-weld studies, where an apparent residual stress decrease is often evident in the steady-state region. The subtler changes in multi-weld scenarios are likely due to the complex interactions of multiple welds within this area,

affecting how stresses are distributed and relieved during the process. These more unique residual stress distributions are probably a function of both temporal and spatial dynamics. When considering the temporal dynamics, the residual stress field of an initial weld is established as it cools and the metal contracts. If a second weld is introduced nearby before the entire structure equilibrates, the heat from the second weld can modify the still-evolving stress field of the first weld. The effect of this modification most likely comes down to its spatial position, where the closer the welds are, the more likely their heat-affected zones will affect each other's stress fields.

Lastly, considering the 160 mm scan line marked by the green line for longitudinal stresses (see Figure 12), this area presents some of the most complex interactions observed in the study. Plate E, a single-welded plate, exhibits a significant increase in residual stress, ranging between 20 to 30 MPa higher than earlier measurements at the 80 mm and 0 mm locations.

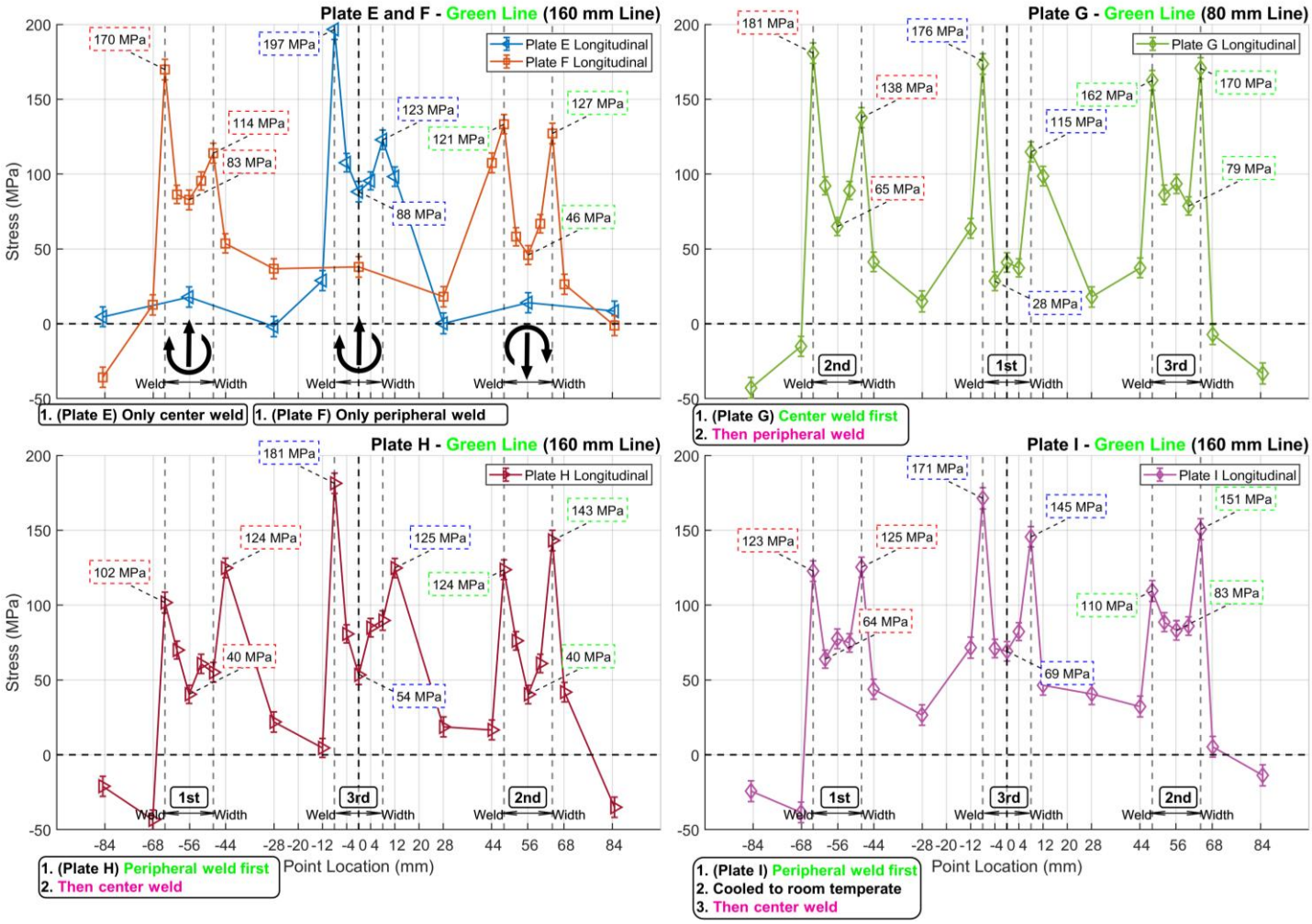


Figure 12: Green line (160 mm line); Stress Direction: Longitudinal

This pattern of high residual stresses at the 160 mm line is consistent across plates G, H, and I, where this line marks the end of the center weld. However, for the peripheral weld, this line coincides with the steady-state region. The welding sequence significantly impacts the residual stresses observed for plates G and H on the 160 mm scan line. Plate G, with the center weld conducted first, shows higher residual stresses at this green scan line before the peripheral weld, resulting in elevated stresses around the periphery. In contrast, Plate H starts with the peripheral weld, which shows lower residual stresses at this line.

However, when the center weld is subsequently performed, it matches or exceeds the stresses seen in Plate G. This suggests that temperature distributions play a crucial role, as evidenced by comparing these plates with Plate F, which only features a peripheral weld starting at the negative 56 mm location. In Plate F, the peripheral weld begins on the colder side of the plate; as it wraps around to the positive 56 mm location, the stresses significantly drop by about 50 MPa.

This decrease may be attributed to either geometric effects or temperature variations influencing the weld's progression. Notably, the end of the peripheral weld in Plates G, H, and I do not show the high residual stresses near the 200 MPa level observed at the center weld's end. This difference is likely due to the peripheral weld's geometry, which does not transition from weld into no-weld or base material as sharply as the center weld. The peripheral weld completes a circuit, ending on itself, which may contribute to a more uniform distribution of stresses and or further release of stress into the geometry as distortion due to the lack of material support on the peripheral welds as they are completed near the plate's edges. The green line, while in a steady state for the peripheral welds, is near the end of the plate for the center weld, capturing the culmination of welding stresses.

In contrast, the closest scan line to the end of the peripheral weld, marked by the blue line, is significantly further away. This is illustrated in Figure 9, at the bottom left of the multi-welded plate, showcasing the exit hole of the peripheral weld. Yet, it does not experience the pronounced ending stresses seen in the center weld, emphasizing the unique impact of the weld's geometrical closure on residual stress distribution. This analysis underscores the importance of considering both the welding sequence and the geometrical configuration of the welds in understanding and predicting residual stress distributions and their potential implications for the structural integrity of welded components.

Examining the transverse stresses is also important, as both types significantly affect the component's structure, integrity, and performance, as well as significantly influence the welded joint's ultimate strength, fatigue life, and fracture toughness. Longitudinal stresses, running along the weld seam, primarily result from thermal expansion and contraction as the tool moves forward and are a common cause of bending. Conversely, transverse stresses occur perpendicular to the weld direction, often due to differential cooling across the weld's width. These stresses are influenced by temperature gradients extending from the advancing and retreating sides of the weld to the HAZ and the base material regions unaffected by the tool's mechanical disturbance. The maximum temperature is typically recorded on the trailing edge of the tool, with maximum temperature gradients originating from this location outward (see Figure 7). Different temperature gradients between these sides are widely acknowledged, as is in the case of the present study (see Figure 7). However, the intensity of the gradient depends on material type, tool design, and welding parameters, to name a few factors. Transverse stresses are critical to consider because, unlike longitudinal stresses, which may lead to cracks along the weld seam, high transverse stresses can cause transverse cracking similar to what was observed by Milan et al. [26]. The transverse stresses are inconsistent throughout the weld, tending to increase towards the end. This increase is highlighted in the comparison between Figure 13 and Figure 14, where Figure 13 represents the start and Figure 14 the end of the weld at the 160-millimeter line, showing an increase in transverse stresses of 20 to 30 MPa, particularly noticeable in the center weld. This pattern is unique to the center weld, demonstrating the plates' varying ability to support stresses near the edges, especially in the transverse direction, extending to the plate's edge more quickly than in the longitudinal direction. Compared to Sabry et al. [13], with similar weld paths but different supporting geometry as the component studied is a battery tray, more uniform transverse

residual stresses were measured across all welds. This uniformity is attributed to the tray's design, featuring a lip that forms a container shape capable of better supporting these stresses and preventing them from converting into distortion.

This geometry suggests that designs incorporating more support can retain higher residual stresses, potentially reducing distortion. The direction and magnitude of these stresses are important in determining how the material will perform under service loads, a key consideration for structural applications where safety and reliability are crucial. Understanding the stress profiles in both directions is vital for designing an optimal welding configuration for the structure. It also informs decisions regarding potential post-weld treatments such as heat treatment, mechanical stress relief processes, or adjustments in the assembly's layout or sequencing of welding paths.

The last direction of consideration, normal stress direction (see Figure 15), typically remains minimal due to modest temperature fluctuations in this orientation and the absence of significant constraints (Williams et al. [10]).

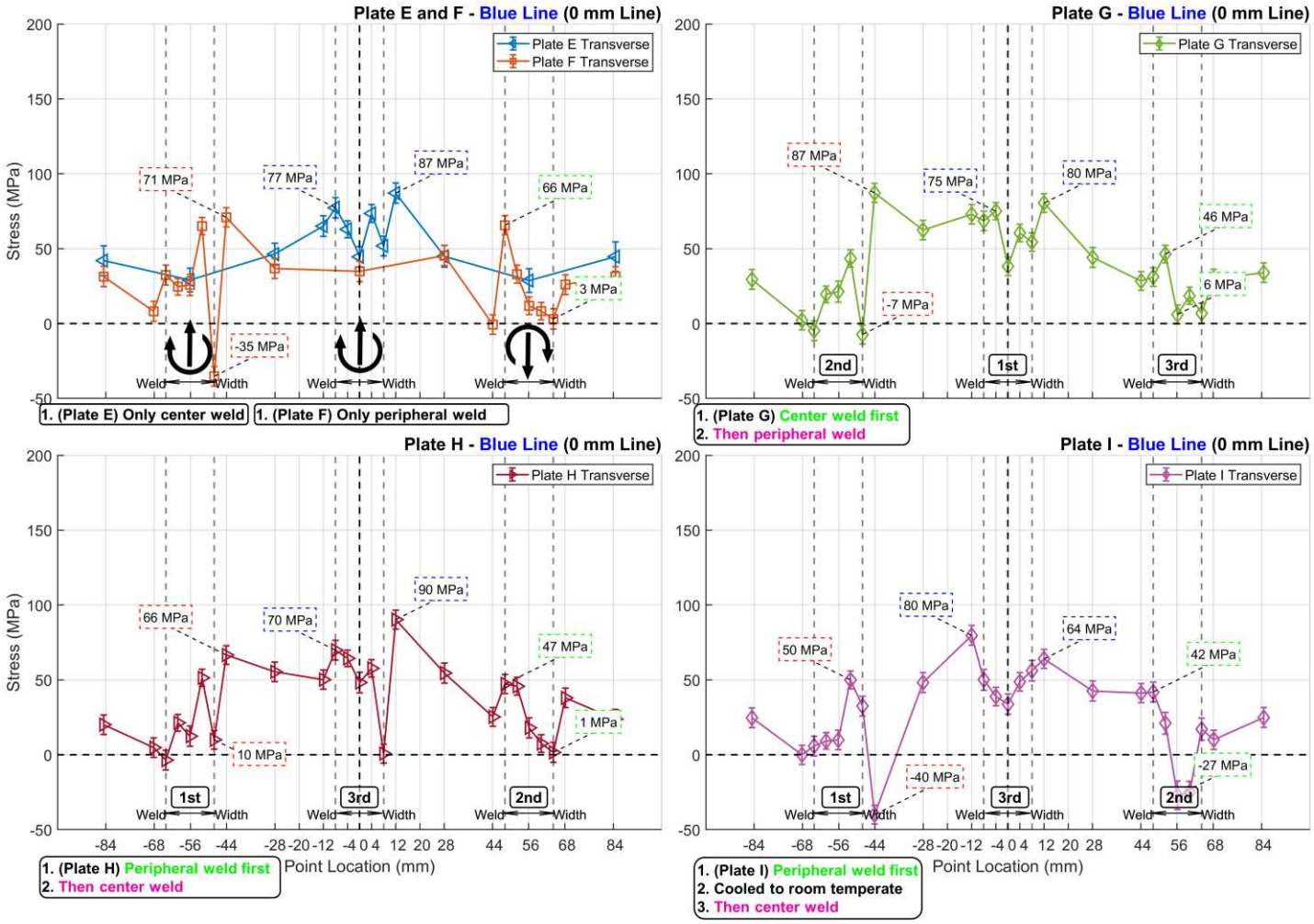


Figure 13: Blue line (0 mm line); Stress Direction: Transverse

Figure 15 encompasses the normal direction of stresses at the 160 mm mark. This direction of stress is by far the most consistent across the start, middle, and end of the weld, with tensile stresses generally not exceeding 55 MPa; therefore, only the ending 160 mm line residual stresses are provided. The most notable feature of the normal profile is the many points near each weld edge exhibit a compressive reaction, underscoring the complex interplay of stresses within welded components. While the normal stress direction shows relatively minimal fluctuations and consistent behavior, this stability is significant as it indicates a relatively uniform thermal profile across the depth of the weld.

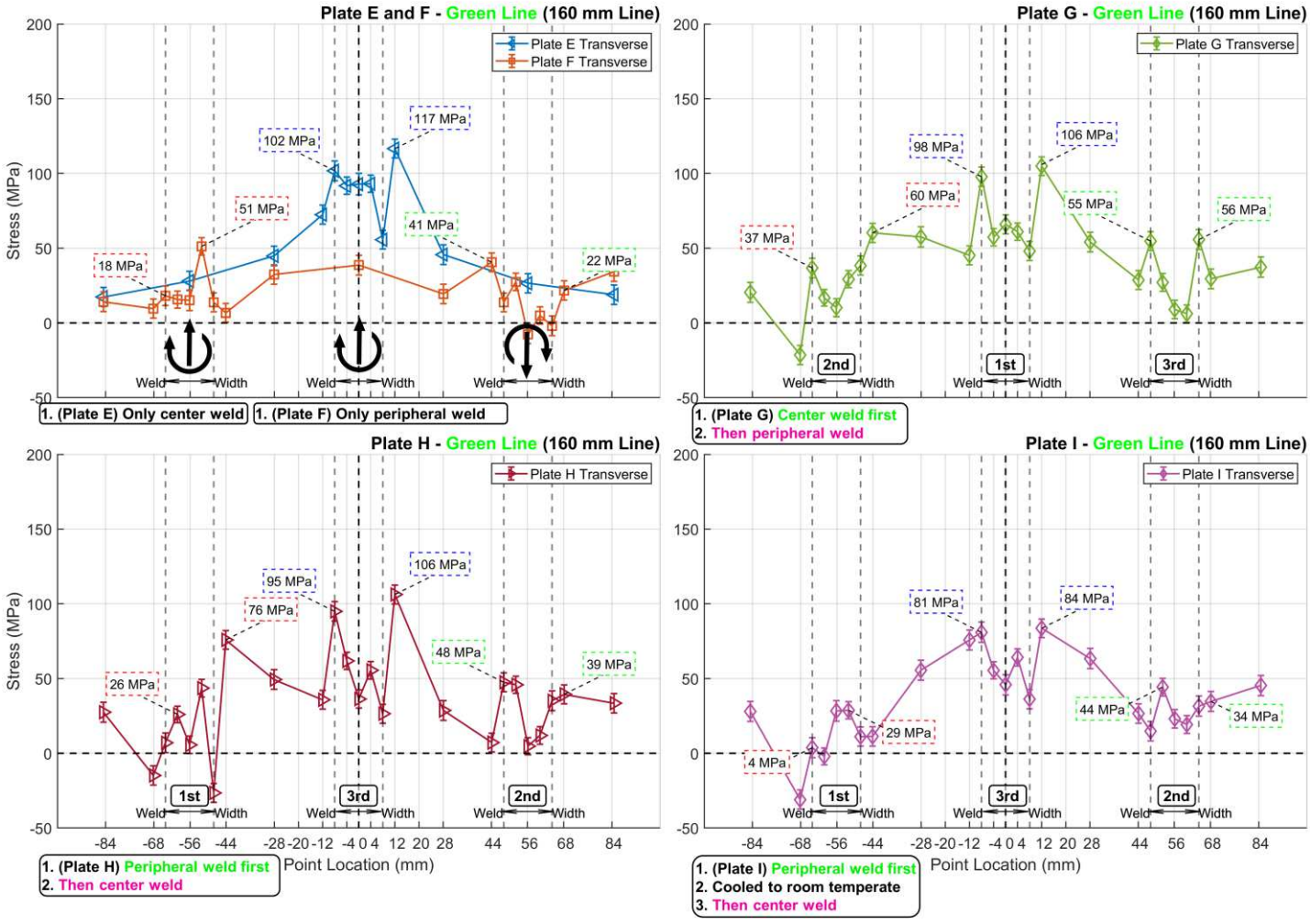


Figure 14: Green line (160 mm line); Stress Direction: Transverse

It is important to consider the plane-stress conditions that exist in the 6061 2 mm plate, especially when evaluating stress distributions away from the weld zones. Plane-stress conditions imply that the stress normal to the plate surface is negligible, while in-plane stresses (longitudinal and transverse) dominate. This assumption is crucial for thin plates like the 2 mm 6061 used in this study, where the thickness is small relative to the other dimensions. However, the observed normal stress of approximately 25 MPa in regions distanced from the weld, as shown in Figure 15, indicates that plane stress conditions might not be perfectly met. This non-zero normal stress

suggests that residual stresses from the welding process are still present and significant, even in regions far from the weld. These residual stresses can contribute to overall distortion and affect the mechanical behavior of the welded component.

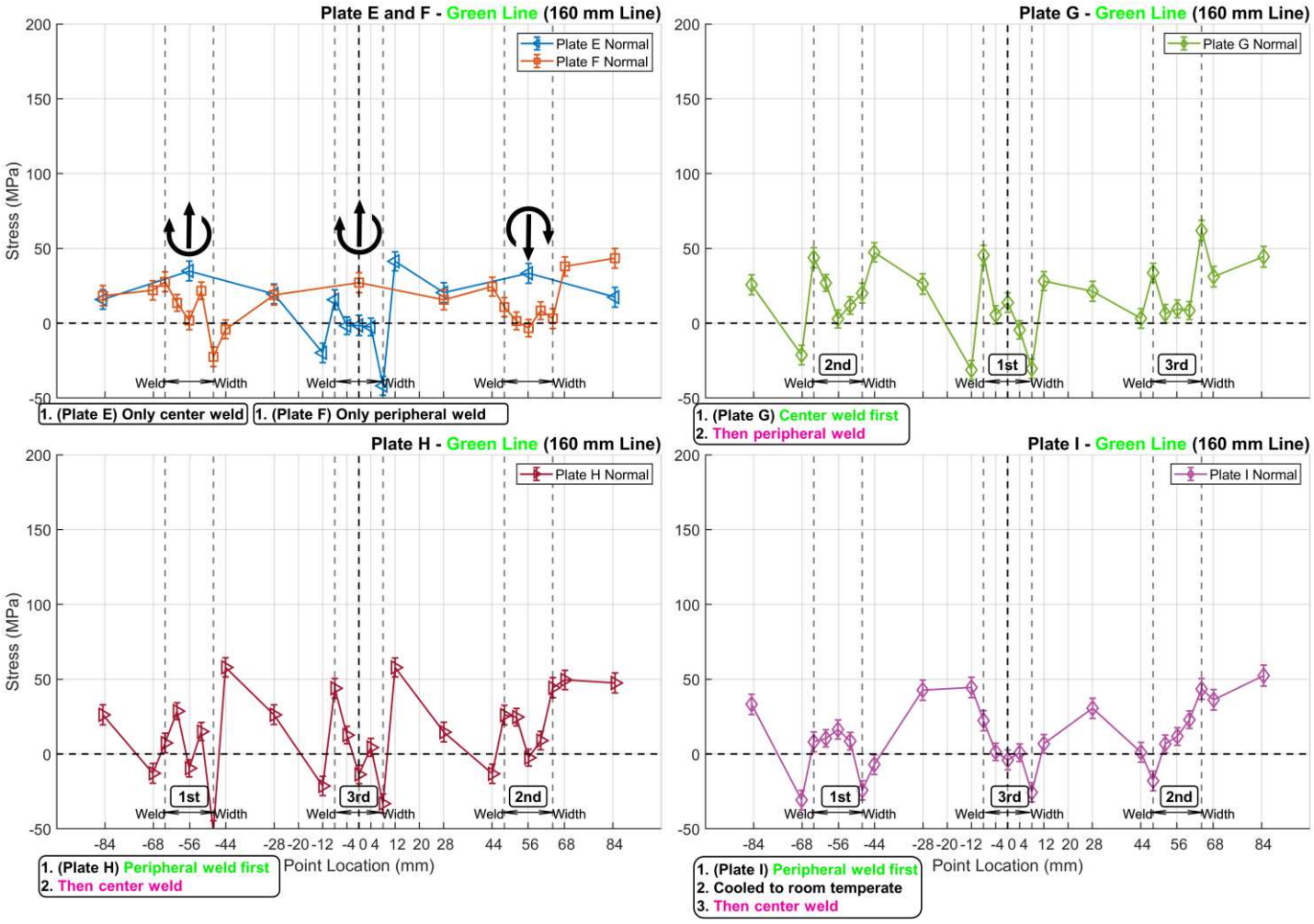


Figure 15: Green line (160 mm line); Stress Direction: Normal

Additionally, many neutron diffraction studies may omit the fabrication of stress-free samples and rely on the plane stress assumption to calculate the d_0 spacing. This study confirms that such an approach may significantly affect the results of neutron diffraction stress scans. Therefore, by ensuring that the plane-stress assumption is valid or by accurately measuring deviations from this condition, one can better predict and mitigate potential distortions and stress concentrations. This

leads to improved weld quality and structural integrity, particularly in thin plates where out-of-plane stresses should ideally be minimized to prevent buckling and other forms of deformation.

4. Conclusions

This study provides a combined experimental and numerical data set integrating neutron diffraction, coordinate-measuring-machine (CMM) distortion mapping, thermocouple measurement, and a validated smoothed-particle-hydrodynamics (SPH) thermal model. Together these characterize how weld sequence and proximity govern residual stress and distortion in multi-welded friction stir welded (FSW) components. A central outcome is that weld sequence and the resulting distortion are partially decoupled: altering the order of welds redistributes the residual stress field yet does not, by itself, change the overall magnitude of distortion. The dominant lever on distortion is instead thermal management, specifically the preservation of heat between successive welds by minimizing wait times. These findings serve as a baseline for simulation and process design in flatness-critical FSW structures such as automotive battery trays. As is typical of neutron-diffraction studies, beam-time allocation limited measurement to a single specimen per weld configuration; the trends reported here are interpreted within that scope. For the aluminum 6061 lap weld to A365 cast structure, the following conclusions are drawn:

(1) The validated SPH model reproduced the measured thermal field and located the maximum temperature (approximately 490 °C, below the 6061 and A365 solidus temperatures of 590 °C and 570 °C) consistently at the trailing edge on the retreating side of the tool. Heat retained from a preceding weld raised the local starting temperature of an adjacent weld by roughly 60 °C, rising from approximately 25 °C to 80 - 100 °C. This altered the contraction behavior during cooling and, in turn, the residual-stress distribution of subsequent welds.

This thermal carryover is the primary mechanism linking weld sequencing to residual stress.

(2) Distortion magnitude is governed by weld length, geometry, and edge material support rather than by weld count alone. A single short center weld (Plate E) produced minimal distortion, localized to approximately −1 mm near the weld exit. In contrast, a single long peripheral weld (Plate F) produced pronounced distortion of approximately −1 mm across the center with corner curling up to +1 mm, owing to its longer weld path and reduced edge support. Distortion then compounds when multiple welds are combined, and increases further when a cooling interval to ambient temperature is introduced between welds (Plate I), which exhibited the largest distortion of all configurations.

(3) Weld sequence alters the residual-stress distribution without changing the resulting distortion magnitude. With sequence as the only variable (Plates G and H), initiating at the center followed by the periphery produced higher tensile residual stresses at the plate edges, whereas beginning at the periphery reduced edge tensile stresses. This redistribution is inferred to benefit edge-region durability, where material support is lowest and crack propagation most likely; however, in the absence of mechanical testing, this remains an inference from the measured stress fields rather than a measured outcome. The benefit is lost when the first weld is allowed to cool before the second (Plate I): the residual-stress field of the cooled first weld dominates, increasing both distortion magnitude and profile change. In practice, welds on a given section of a large component should therefore be completed in rapid succession to preserve inter-weld heat.

(4) Longitudinal residual stress was the largest stress component measured. Peak longitudinal stress reached approximately 180 MPa at the advancing-side TMAZ/HAZ interface,

coinciding with the local (weld-softened) yield strength, above which further thermo-mechanical load is released as plastic deformation. The profiles displayed the asymmetric "M" shape characteristic of FSW, with advancing-to-retreating differences up to approximately 50 MPa. Central welds terminating in base material exhibited the highest longitudinal stresses, approaching 200 MPa at the weld end, whereas peripheral welds closing on themselves showed lower and more uniform stresses. Transverse stresses increased from weld start to weld end by approximately 20 - 30 MPa and were most pronounced in central welds; peripheral welds, lacking edge material support, exhibited significantly lower or compressive stresses. These trends indicate that support geometry and weld closure, rather than sequence alone, control the multi-directional stress state.

(5) Neutron-diffraction stress determination that omits fabricated stress-free (d_0) reference samples and relies instead on the plane-stress assumption can misestimate the stress state. A non-zero normal stress of approximately 25 MPa was measured in regions remote from the weld, and interacting welds generated normal tensile stresses of roughly 50 MPa in the base material, indicating that the plane-stress assumption is not strictly satisfied even in the thin (2 mm) 6061 sheet. Fabricating stress-free samples for each material zone is therefore recommended for accurate residual-stress measurement in multi-welded thin-plate FSW.

5. CRediT Author Statement

Nicholas Sabry: Methodology, Formal analysis, Investigation, Writing – original draft, Visualization. Dimitry Sediako: Conceptualization, Methodology, Resources, Writing – review & editing, Supervision, Funding acquisition. Kirk Fraser: Conceptualization, Methodology, Resources, Writing – review & editing. Francois Nadeau: Conceptualization, Methodology, Resources, Writing – review & editing. Joshua Stroh: Investigation, Supervision, Writing – review

& editing. Anna Paradowska: Methodology, Resources, Supervision. Mark Reid: Methodology, Resources, Supervision, Writing – review & editing.

Acknowledgments

The authors extend their gratitude to the National Research Council (NRC) for their support in the FSW procedure and for providing the materials used in this study. Additionally, they would like to thank the Australian Nuclear Science and Technology Organisation (ANSTO) and the Australian Centre for Neutron Scattering (ACNS) for conducting the neutron diffraction experiments, under proposal numbers P16496 and P16494. Special thanks go to Jordan Kozakevich for his significant contribution to developing the custom casting process that enabled the creation of the A365 plate geometries used in the welding.

Funding

This research did not receive any specific grant from funding agencies in the public, commercial, or not-for-profit sectors.

Statements and Declarations

Competing interests: The authors have no relevant financial or non-financial interests to disclose.

Data Availability

The research data that validate the findings of this study have been deposited in Mendeley Data and can be accessed at https://doi.org/10.17632/mnffnr63kf.1

6. References

[1] S. Bhardwaj, S.K. Aas, R.M.C. Ratnayake, Experimental and numerical investigation of residual stresses in proximity girth welds, Int. J. Adv. Manuf. Technol. 126 (2023) 1247–1259. https://doi.org/10.1007/s00170-023-11162-1.

[2] S. Sun, J. Wang, B. Gao, G. Cao, S. Zhang, Influence of Friction Stir Weld Seam Distribution on Spun Formed Workpieces, Int. J. Precis. Eng. Manuf. 25 (2024) 1183–1194. https://doi.org/10.1007/s12541-024-00994-w.

[3] J.P. Martin, C. Stanhope, S. Gascoyne, Novel techniques for corner joints using friction stir welding, TMS Annu. Meet. (2011) 179–186. https://doi.org/10.1002/9781118062302.ch22.

[4] J.S. Agapiou, B.E. Carlson, Friction stir welding for assembly of copper squirrel cage rotors for electric motors, Procedia Manuf. 48 (2020) 1143–1154. https://doi.org/10.1016/j.promfg.2020.05.156.

[5] C. Dalle Donne, G. Biallas, T. Ghidini, G. Raimbeaux, Effect of Weld Imperfections and Residual Stresses on the Fatigue Crack Propagation in Friction Stir Welded Joints, in: Second Int. Conf. Frict. Stir Welding, 2000. https://doi.org/10.1520/JAI12036.

[6] C.M. Chen, R. Kovacevic, Parametric finite element analysis of stress evolution during friction stir welding, Proc. Inst. Mech. Eng. Part B J. Eng. Manuf. 220 (2006) 1359–1371. https://doi.org/10.1243/09544054JEM324.

[7] C.A. Charitidis, D.A. Dragatogiannis, E.P. Koumoulos, I.A. Kartsonakis, Residual stress and deformation mechanism of friction stir welded aluminum alloys by nanoindentation, Mater. Sci. Eng. A. 540 (2012) 226–234. https://doi.org/10.1016/j.msea.2012.01.129.

[8] M.I. Costa, C. Leitão, D.M. Rodrigues, Parametric study of friction stir welding induced distortion in thin aluminium alloy plates: A coupled numerical and experimental analysis, Thin-Walled Struct. 134 (2019) 268–276. https://doi.org/10.1016/j.tws.2018.10.027.

[9] X. Xu, H. Yu, Z. Lin, Study of residual stress variation with depth of friction stir welded

aluminium plates with different thicknesses, Sci. Technol. Weld. Join. 25 (2020) 297–302. https://doi.org/10.1080/13621718.2019.1693722.

[10] S.W. Williams, A. Steuwer, Residual stresses in friction stir welding, Woodhead Publishing Limited, 2009. https://doi.org/10.1533/9781845697716.2.215.

[11] P. Staron, M. Koçak, S. Williams, A. Wescott, Residual stress in friction stir-welded A1 sheets, Phys. B Condens. Matter. 350 (2004) 491–493. https://doi.org/10.1016/j.physb.2004.03.128.

[12] W. He, J. Liu, W. Hu, G. Wang, W. Chen, Controlling residual stress and distortion of friction stir welding joint by external stationary shoulder, High Temp. Mater. Process. 38 (2019) 662–671. https://doi.org/10.1515/htmp-2019-0005.

[13] N. Sabry, J. Stroh, D. Sediako, G. Byczynski, A. Lombardi, A. Payzant, Stress characterization for friction-stir-welded electric vehicle battery trays with application of neutron diffraction, J. Manuf. Process. 101 (2023) 1109–1123. https://doi.org/10.1016/j.jmapro.2023.06.035.

[14] P. Shahi, M. Barmouz, P. Asadi, Force and torque in friction stir welding, Woodhead Publishing Limited, 2014. https://doi.org/10.1533/9780857094551.459.

[15] P.C. Sinclair, W.R. Longhurst, C.D. Cox, D.H. Lammlein, A.M. Strauss, G.E. Cook, Heated friction stir welding: An experimental and theoretical investigation into how preheating influences process forces, Mater. Manuf. Process. 25 (2010) 1283–1291. https://doi.org/10.1080/10426914.2010.496122.

[16] B. Meyghani, C. Wu, Progress in Thermomechanical Analysis of Friction Stir Welding, Chinese J. Mech. Eng. (English Ed. 33 (2020). https://doi.org/10.1186/s10033-020-0434-7.

[17] M.E. Sigl, A. Bachmann, T. Mair, M.F. Zaeh, Torque-based temperature control in friction stir welding by using a digital twin, Metals (Basel). 10 (2020) 1–18. https://doi.org/10.3390/met10070914.

[18] K. Fraser, Robust and efficient meshfree solid thermo-mechanics simulation of friction stir welding, Université du Québec à Chicoutimi, UQAC, 2017.

[19] A. Silva-Magalhães, J. De Backer, J. Martin, G. Bolmsjö, In-situ temperature measurement in friction stir welding of thick section aluminium alloys, J. Manuf. Process. 39 (2019) 12–17. https://doi.org/10.1016/j.jmapro.2019.02.001.

[20] C.K. Jin, Microstructures and Mechanical Properties of A356 Alloy and A6061 Alloy through Rheo, Upsetting, Thixo, Forming Process, and T6 Heat Treatment, Metals (Basel). 12 (2022). https://doi.org/10.3390/met12122051.

[21] F.C.B.C. Hernandez, J.H. Sokolowski, J.J. De Cruz Rivera, Micro-Raman analysis of the Si particles present in Al-Si hypereutectic alloys in liquid and semi-solid states, Adv. Eng. Mater. 9 (2007) 46–51. https://doi.org/10.1002/adem.200600173.

[22] W. Tang, X. Guo, J.C. McClure, L.E. Murr, A. Nunes, Heat input and temperature distribution in friction stir welding, J. Mater. Process. Manuf. Sci. 7 (1998) 163–172. https://doi.org/10.1106/55TF-PF2G-JBH2-1Q2B.

[23] N. Sabry, Development of Friction Stir Welding on Large Multi-Welded Components: Residual Stress, Distortion, and Crystallographic Texture in Lap Joints of Aluminum Alloys, The University of British Columbia, 2024. https://doi.org/https://dx.doi.org/10.14288/1.0444948.

[24] N. Sabry, J. Stroh, D. Sediako, Characterization of microstructure and residual stress following the friction stir welding of dissimilar aluminum alloys, CIRP J. Manuf. Sci. Technol. 41 (2023) 365–379. https://doi.org/10.1016/j.cirpj.2022.11.021.

[25] D. Radaj, Heat Effects of Welding, 1992. https://doi.org/10.1007/978-3-642-48640-1.

[26] M.T. Milan, W.W. Bose Filho, J.R. Tarpani, Fatigue crack growth behavior of friction stir welded 2024-T3 aluminum alloy tested under accelerated salt fog exposure, Mater. Perform. Charact. 3 (2014) 232–251. https://doi.org/10.1520/MPC20130036.